Transient thermal response of a functionally graded piezoelectric laminate with a crack normal to the bimaterial interface

Y.Nakaue[1] **and S. Ueda**[2]

[1, 2] Department of Mechanical Engineering, Osaka Institute of Technology,
5-16-1 Omiya, Asahi-ku, Osaka 535-8585, Japan

[1] Presenting author: n.yoshihisa.oit@gmail.com
[2] Corresponding author: sei.ueda@oit.ac.jp

Abstract

In this paper, the fracture problem of a functionally graded piezoelectric material strip (FGPM strip) containing a crack perpendicular to the interface between an FGPM strip and a homogeneous layer is considered. The problem is solved for the laminate that is suddenly heated from the surface of the FGPM strip. The surface of the homogeneous layer is maintained at the initial temperature. The crack faces are supposed to be completely insulated. Material properties are assumed to be exponentially dependent on the distance from the interface. By using the Laplace and Fourier transforms, the thermo-electro-mechanical fracture problem is reduced to a singular integral equation, which is solved numerically. The stress intensity factors are computed and presented as a function of the normalized time, the nonhomogeneous and geometric parameters.

Keywords: functionally graded piezoelectric material, fracture mechanics, stress intensity factor, elasticity

Introduction

The concept of the well-known functionally graded materials (FGMs) can be extended to the piezoelectric material to improve its reliability [1]. As a result, it is also important to investigate the fracture behavior of functionally graded piezoelectric materials (FGPMs) under thermal load, and some interesting results have been reported. For example, Wang and Noda [2] treated the thermally induced fracture of a smart functionally graded composite structure. The present author has investigated the singular fields around cracks in FGPMs under the static thermal loading condition [3-5] and under the thermal shock loading condition [6-8]. It was found that by selecting the material constants appropriately, the steady stress and electric displacement intensity factors can be lowered substantially. Moreover, the overshooting phenomenon of the stress and electric displacement intensity factors was observed in a homogeneous piezoelectric strip [9, 10] and in an FGPM strip [6-8].

On the other hand, piezoelectric composites have been used in a wide variety of applications including vibration control and actuators. These systems can be achieved by incorporating a thin piezoelectric layer into a structural system. Several kinds of piezoelectric actuators have been designed. Uchino et al. [11] fabricated a monomorph actuator made from semi-conductive piezoelectric ceramics.

In this paper, we focused on the transient thermal fracture problem of monomorph actuators using an FGPM strip. The analytical model of the monomorph actuator consists of an FGPM strip and a homogeneous elastic layer. The problem of the normal crack in the FGPM strip is analyzed under transient thermal loading conditions. Material properties are exponentially dependent on the distance from the interface between the FGPM strip and the homogeneous elastic layer. The superposition technique is used to solve the governing equations. The transient temperature and transient thermal stress in an un-cracked FGPM strip are calculated by the Laplace transform, and a numerical method is employed to obtain time-dependent solutions by way of a Laplace inversion technique [12]. The obtained thermal stress is used as the crack surface tractions with opposite sign to formulate the mixed boundary value problem. By using the Fourier transform techniques [13, 14], the electromechanical problem is reduced to a singular integral equation, which are solved numerically [15]. The stress intensity factors are computed and presented as functions of the normalized time, the nonhomogeneous and geometric parameters.

Formulation of the problem

Consider a strip of FGPM of thickness h_1 containing a finite crack bonded to an elastic layer of thickness h_2 with the rectangular Cartesian coordinate system (x, y, z) as shown in Figure 1. The crack of length $2c$ is located along z-axis from a to b $(b-a=2c, \quad 0<a<b<h_1)$. The piezoelectric strip is poled in the z-direction and is in the plane strain conditions perpendicular to the y-axis. It is assumed that initially the medium is at the uniform temperature T_I and is suddenly subjected to a uniform temperature rise $T_0H(t)$ along the boundary $z=h_1$, where $H(t)$ is the Heaviside step function and t denotes time. The temperature along the boundary $z=-h_2$ is maintained at T_I. The crack faces remain thermally and electrically insulated.

The material property parameters are taken to vary continuously along the z-direction inside the FGPM strip. The material properties of FGPM, such as the elastic stiffness constants $c_{kl}(z)$, the piezoelectric constants $e_{kl}(z)$, the dielectric constants $\varepsilon_{kk}(z)$, the stress-temperature coefficients $\lambda_{kk}(z)$, the coefficient of heat conduction $\kappa_x(z), \kappa_z(z)$ and the pyroelectric constant $p_z(z)$, are one-dimensionally dependent as

$$\left.\begin{aligned}
&(c_{kl}, e_{kl}, \varepsilon_{kk}) = (c_{kl0}, e_{kl0}, \varepsilon_{kk0})\exp(\beta z)\\
&(\lambda_{kk}, p_z) = (\lambda_{kk0}, p_{z0})\exp[(\beta+\omega)z]\\
&(\kappa_x, \kappa_z) = (\kappa_{x0}, \kappa_{z0})\exp(\delta z)
\end{aligned}\right\} \tag{1}$$

where β, ω and δ are positive or negative constants, and the subscript 0 indicates the properties at the plane $z=0$. For some materials, the thermal diffusivity τ_0 indeed doesn't vary dramatically, then τ_0 is assumed to be a constant. The material properties of the homogeneous elastic layer are the elastic stiffness constants c_{kl}^E, the stress-temperature coefficients λ_{kk}^E, the coefficient of heat conduction κ^E and the thermal diffusivity τ_0^E. The superscript E denotes the physical quantities of the homogeneous elastic layer.

The crack problem may be solved by superposition. In the problem considered here, since the heat conduction is one-dimensional and straight cracks do not obstruct the heat flow in this arrangement, determination of the temperature distribution and the resulting thermal stress would be quite straightforward and the related crack problem would be one of model I. We suppose that each crack is opened under the action of the same distribution of the internal pressure $\sigma_0^T(z,t)$, where $\sigma_0^T(z,t)$ is the thermal stress induced by the time-dependent temperature change. In the following, the subscripts x, y, z will be used to refer to the direction of coordinates.

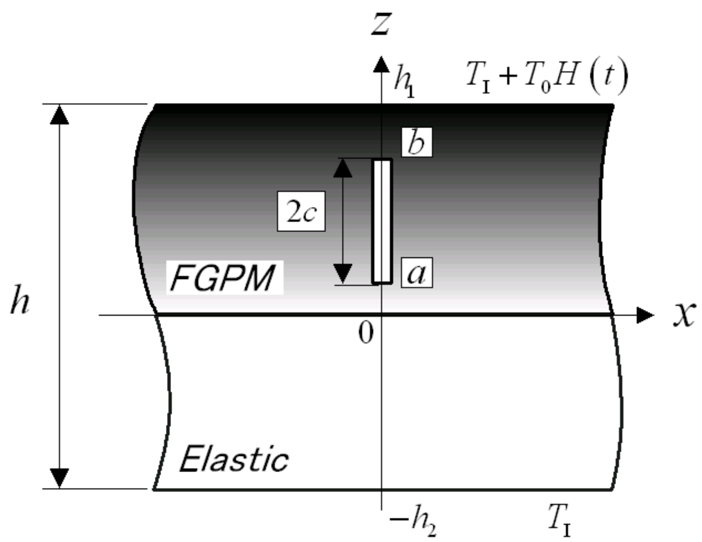

Figure 1 : Geometry of the crack problem in a functionally graded piezoelectric laminate

Temperature distribution and thermal stress in the un-cracked strip

By using the Laplace transform method, the temperatures $T^*(z,p) \quad (0 \le z \le h_1)$ and $T^{E*}(z,p) \quad (-h_2 \le z \le 0)$ in the Laplace transform plane can be easily obtained as follows:

$$\left.\begin{aligned} T^*(z,p) &= \sum_{j=1}^{2} D_{1j} \exp(\mu_{1j} z) \quad (0 \le z \le h_1) \\ T^{E*}(z,p) &= \sum_{j=1}^{2} D_{2j} \exp(\mu_{2j} z) \quad (-h_2 \le z \le 0) \end{aligned}\right\} \tag{2}$$

where the superscript $*$ denotes the physical quantities in the Laplace domain and p is the Laplace parameter. The functions μ_{ij} and D_{ij} $(i, j = 1, 2)$ are given in Appendix A. Thus the temperature fields $T(z,t)$ $(0 \le z \le h_1)$ and $T^E(z,t) \quad (-h_2 \le z \le 0)$ in the time domain may be evaluated as:

$$\left.\begin{aligned} T(z,t) &= \frac{1}{2\pi i}\int_{Br} T^*(z,p)\exp(pt)dp \quad (0 \le z \le h_1) \\ T^E(z,t) &= \frac{1}{2\pi i}\int_{Br} T^{E*}(z,p)\exp(pt)dp \quad (-h_2 \le z \le 0) \end{aligned}\right\} \tag{3}$$

The temperature fields $T(z,t)$ $(0 \le z \le h_1)$ and $T^E(z,t)$ $(-h_2 \le z \le 0)$ can be found from Eq. (3) by using the numerical Laplace inversion scheme [12].

Once $T(z,t)\,(0 \le z \le h_1)$ and $T^E(z,t)\,(-h_2 \le z \le 0)$ is known, the thermal stress component $\sigma_{xx}^T(z,t)\,(0 \le z \le h_1)$ can be also obtained by the following equation:

$$\sigma_{xx}^T = \bar{c}_{110}\exp(\beta z)\frac{\partial u_x^T}{\partial x} - \bar{\lambda}_{110}\exp[(\beta+\omega)z]T \tag{4}$$

where the superscript T denotes the thermally induced quantities, $u_x^T(z,t)$ is the displacement component and

$$\left.\begin{aligned}
\bar{c}_{110} &= c_{110} - \frac{c_{130}(c_{130}\varepsilon_{330} + e_{310}e_{330}) + e_{310}(c_{130}e_{330} - c_{330}e_{310})}{c_{330}\varepsilon_{330} + e_{330}^2} \\
\bar{\lambda}_{110} &= \lambda_{110} - \frac{\lambda_{330}(c_{130}\varepsilon_{330} + e_{310}e_{330}) - p_{z0}(c_{130}e_{330} - c_{330}e_{310})}{c_{330}\varepsilon_{330} + e_{330}^2}
\end{aligned}\right\} \tag{5}$$

Similarly, $\sigma_{xx}^{ET}(z,t)\,(-h_2 \le z \le 0)$ is given by

$$\sigma_{xx}^{ET} = \bar{c}_{11}^E\frac{\partial u_x^{ET}}{\partial x} - \bar{\lambda}_{11}^E T^E \tag{6}$$

where $u_x^{ET}(z,t)$ is the displacement component and

$$\bar{c}_{11}^E = c_{11}^E - \frac{\left(c_{13}^E\right)^2}{c_{33}^E}, \quad \bar{\lambda}_{11}^E = \lambda_{11}^E - \frac{c_{13}^E\lambda_{33}^E}{c_{33}^E} \tag{7}$$

The compatibility conditions that need to be satisfied become

$$\frac{\partial^2}{\partial z^2}\left[\frac{\partial u_x^T}{\partial x}\right] = 0, \quad \frac{\partial^2}{\partial z^2}\left[\frac{\partial u_x^{ET}}{\partial x}\right] = 0 \tag{8}$$

giving

$$\left.\begin{aligned}&\frac{\partial u_x^T}{\partial x}=A^T z+B^T\\&\sigma_{xx}^T=\bar{c}_{110}\exp(\beta z)(A^T z+B^T)-\bar{\lambda}_{110}\exp[(\beta+\omega)z]T\end{aligned}\right\} \tag{9}$$

$$\left.\begin{aligned}&\frac{\partial u_x^{ET}}{\partial x}=A^T z+B^T\\&\sigma_{xx}^{ET}=\bar{c}_{11}^E(A^T z+B^T)-\bar{\lambda}_{11}^E T^E\end{aligned}\right\} \tag{10}$$

where $A^T(t)$ and $B^T(t)$ are unknown functions to be obtained from boundary conditions for the laminate. If the laminate is unconstrained along its boundaries, we have

$$\left.\begin{aligned}&\int_0^{h_1}\sigma_{xx}^T(z,t)dz+\int_{-h_2}^0\sigma_{xx}^{ET}(z,t)dz=0\\&\int_0^{h_1}\sigma_{xx}^T(z,t)zdz+\int_{-h_2}^0\sigma_{xx}^{ET}(z,t)zdz=0\end{aligned}\right\} \tag{11}$$

In the crack problem under considered, the equal and opposite of the stress $\sigma_0^T(z,t)=\sigma_{xx}^T(z,t)\quad(a<z<b)$ given by Eq. (4) will be used as the crack surface traction and the laminate will be assumed to be under plane-strain conditions.

The crack problem

Referring to Figure 1, it is assumed that $x=0$ is a plane of symmetry regarding to geometry and loading conditions. Thus, in analyzing the problem it is sufficient to consider one-half ($0\le x<\infty$) of the FGPM strip and the homogeneous elastic layer only. Also, through a proper superposition, the problem is assumed to have been reduced to a perturbation problem in which the crack surface tractions are the only nonzero external loads and the stresses in the layered strip vanish for $x\to\infty$.

Taking Eqs. (1) into consideration, the governing equations for the electromechanical fields of the FGPM strip and the homogeneous elastic layer may then be expressed as follows:

$$\left.\begin{aligned}
&c_{110}\frac{\partial^2 u_x}{\partial x^2}+c_{440}\frac{\partial^2 u_x}{\partial z^2}+\left(c_{130}+c_{440}\right)\frac{\partial^2 u_z}{\partial x\partial z}+\left(e_{310}+e_{150}\right)\frac{\partial^2 \phi}{\partial x\partial z}\\
&\qquad+\beta\left\{c_{440}\left(\frac{\partial u_x}{\partial z}+\frac{\partial u_z}{\partial x}\right)+e_{150}\frac{\partial \phi}{\partial x}\right\}=0\\
&c_{440}\frac{\partial^2 u_z}{\partial x^2}+c_{330}\frac{\partial^2 u_z}{\partial z^2}+\left(c_{130}+c_{440}\right)\frac{\partial^2 u_x}{\partial x\partial z}+e_{150}\frac{\partial^2 \phi}{\partial x^2}+e_{330}\frac{\partial^2 \phi}{\partial z^2}\\
&\qquad+\beta\left(c_{130}\frac{\partial u_x}{\partial x}+c_{330}\frac{\partial u_z}{\partial z}+e_{330}\frac{\partial \phi}{\partial z}\right)=0\\
&e_{150}\frac{\partial^2 u_z}{\partial x^2}+e_{330}\frac{\partial^2 u_z}{\partial z^2}+\left(e_{150}+e_{310}\right)\frac{\partial^2 u_x}{\partial x\partial z}-\varepsilon_{110}\frac{\partial^2 \phi}{\partial x^2}-\varepsilon_{330}\frac{\partial^2 \phi}{\partial z^2}\\
&\qquad+\beta\left(e_{310}\frac{\partial u_x}{\partial x}+e_{330}\frac{\partial u_z}{\partial z}-\varepsilon_{330}\frac{\partial \phi}{\partial z}\right)=0
\end{aligned}\right\} \tag{12}$$

$$\left.\begin{aligned}
c_{11}^E\frac{\partial^2 u_x^E}{\partial x^2}+c_{44}^E\frac{\partial^2 u_x^E}{\partial z^2}+\left(c_{13}^E+c_{44}^E\right)\frac{\partial^2 u_z^E}{\partial x\partial z}=0\\
c_{44}^E\frac{\partial^2 u_z^E}{\partial x^2}+c_{33}^E\frac{\partial^2 u_z^E}{\partial z^2}+\left(c_{13}^E+c_{44}^E\right)\frac{\partial^2 u_x^E}{\partial x\partial z}=0
\end{aligned}\right\} \tag{13}$$

The boundary conditions can be written as

$$\left.\begin{aligned}
&\sigma_{xx}(0,z,t)=-\sigma_0^T(z,t) && (a<z<b)\\
&u_x(0,z,t)=0 && (0\le z\le a,\, b\le z\le h_1)
\end{aligned}\right\} \tag{14}$$

$$\left.\begin{aligned}
\sigma_{zx}(0,z,t)=0\\
D_x(0,z,t)=0
\end{aligned}\right\}\quad (0\le z\le h_1) \tag{15}$$

$$\left.\begin{aligned}
\sigma_{zx}^E(0,z,t)=0\\
u_x^E(0,z,t)=0
\end{aligned}\right\}\quad (-h_2\le z\le 0) \tag{16}$$

$$\left.\begin{aligned}
\sigma_{zx}(x,h_1,t)=0\\
\sigma_{zz}(x,h_1,t)=0\\
D_z(x,h_1,t)=0
\end{aligned}\right\}\quad (0\le x<\infty) \tag{17}$$

$$\left.\begin{array}{l}\sigma_{zx}(x,0,t)=\sigma_{zx}^{E}(x,0,t)\\ \sigma_{zz}(x,0,t)=\sigma_{zz}^{E}(x,0,t)\\ D_z(x,0,t)=0\\ u_x(x,0,t)=u_x^{E}(x,0,t)\\ u_z(x,0,t)=u_z^{E}(x,0,t)\end{array}\right\}\quad (0\le x<\infty) \tag{18}$$

$$\left.\begin{array}{l}\sigma_{zx}^{E}(x,-h_2,t)=0\\ \sigma_{zz}^{E}(x,-h_2,t)=0\end{array}\right\}\quad (0\le x<\infty) \tag{19}$$

By using the Fourier integral transform technique, the stress intensity factors $K_{\mathrm{IA}}(t)$ at $z=a$ and $K_{\mathrm{IB}}(t)$ at $z=b$ may be evaluated as

$$K_{\mathrm{IA}}(t)=\left\{\begin{array}{ll}-Z^{\infty}\exp(\beta a)(\pi c)^{1/2}\Phi(a,t) & (b<h_1)\\ \\ -Z^{\infty}\exp(\beta a)(4\pi c)^{1/2}\Phi(a,t) & (b=h_1)\end{array}\right\} \tag{20}$$

$$K_{\mathrm{IB}}(t)=\left\{\begin{array}{ll}Z^{\infty}\exp(\beta b)(\pi c)^{1/2}\Phi(b,t) & (b<h_1)\\ \\ 0 & (b=h_1)\end{array}\right\} \tag{21}$$

In Eqs.(20) and (21), the constant Z^{∞} is given in Appendix B and the function $\Phi(u,t)$ is given by

$$G(\xi,t)=\frac{\Phi(u,t)}{(1+u)^{1/2}(1-u)^{\alpha}} \tag{22}$$

where $\alpha=1/2$ for $0<b<h_1$ (embedded crack) and $\alpha=-1/2$ for $b=h_1$ (edge crack), and $\xi=(b-a)u/2+(b+a)/2$. The function $G(\xi,t)$ is the solution of the following singular integral equation obtained from the mixed boundary conditions (14) with the boundary conditions (15)-(19).

$$\int_a^b G(\xi,t)\left[\frac{1}{\xi-z}+\sum_{i=1}^{4}M_i(\xi,z)\right]d\xi=\exp(-\beta z)\frac{\pi}{\Re[Z^{\infty}]}\sigma_0^{T}(z,t)\quad (a<z<b) \tag{23}$$

In the integral equation, the kernel functions $M_i(\xi,t)\ (i=1,2,3,4)$ are also given in Appendix B. The singular integral equation (23) for $0<b<h_1$ (embedded crack) is to be solved with the following subsidiary conditions obtained from the second mixed boundary condition of Eqs.(14).

$$\int_a^b G(\xi,t)d\xi = 0 \tag{24}$$

Numerical result and discussion

For the numerical calculations, the properties of cadmium selenide [16] are used as the properties of the FGPM strip at the plane $z=0$.

$$\left.\begin{array}{ll} c_{110} = 7.41\times10^{10}[\mathrm{N/m^2}], & c_{130} = 3.93\times10^{10}[\mathrm{N/m^2}], \\ c_{330} = 8.36\times10^{10}[\mathrm{N/m^2}], & c_{440} = 1.32\times10^{10}[\mathrm{N/m^2}], \\ e_{310} = -0.16[\mathrm{C/m^2}], & e_{330} = 0.347[\mathrm{C/m^2}], \\ e_{150} = -0.138[\mathrm{C/m^2}], & \\ \varepsilon_{110} = 0.825\times10^{-10}[\mathrm{C/Vm}], & \varepsilon_{330} = 0.903\times10^{-10}[\mathrm{C/Vm}], \\ \lambda_{110} = 0.621\times10^{6}[\mathrm{N/Km^2}], & \lambda_{330} = 0.551\times10^{6}[\mathrm{N/Km^2}], \\ p_{z0} = -2.94\times10^{-6}[\mathrm{C/Km^2}]. & \end{array}\right\} \tag{25}$$

Since the values of the coefficients of heat conduction for cadmium selenide could not be found in the literature, the value $\kappa^2 = \kappa_x/\kappa_z = 1/1.5$ is used. The normalized nonhomogeneous parameters βh_1, ωh_1, δh_1 and the thermal diffusivities τ_0 and $\tau_0{}^E$ are assumed to be $\beta h_1 = \omega h_1 = \delta h_1$ and $\tau_0 = \tau_0{}^E$. The properties of titanium (Ti) and brass with following properties are also used as the properties of the elastic layer.

$$\left.\begin{array}{ll} c_{11}^E = c_{33}^E = \dfrac{2(1-\nu)}{1-2\nu}\mu, & c_{13}^E = \dfrac{2\nu}{1-2\nu}\mu, \\ c_{44}^E = \mu, & \lambda_{11}^E = \lambda_{33}^E = \dfrac{2(1+\nu)}{1-2\nu}\mu\alpha^E. \end{array}\right\} \tag{26}$$

where α^E is the coefficient of linear thermal expansion. The values of μ, ν and α^E of titanium (Ti) and brass are

$$\left.\begin{array}{l} \mu = \begin{cases} 42.6\times10^9\ [\mathrm{N/m^2}] & (\mathrm{Ti}) \\ 41.4\times10^9\ [\mathrm{N/m^2}] & (\mathrm{Brass}) \end{cases} \\ \nu = \begin{cases} 0.28 & (\mathrm{Ti}) \\ 0.33 & (\mathrm{Brass}) \end{cases} \\ \alpha^E = \begin{cases} 8.4\times10^{-6}\ [1/\mathrm{K}] & (\mathrm{Ti}) \\ 19.9\times10^{-6}\ [1/\mathrm{K}] & (\mathrm{Brass}) \end{cases} \end{array}\right\} \tag{27}$$

First of all, we consider the effect of the thickness ratio h_2 / h_1 on the stress intensity factors K_{IA} and K_{IB} for the Ti elastic layer. Figures 2(a) and 2(b) show the normalized stress intensity factors $(K_{\mathrm{IA}},\, K_{\mathrm{IB}}) / \lambda_{110} T_0 (\pi c)^{1/2}$ versus time t for $h_2 / h_1 = 1.0$, 0.5 and $\rightarrow 0.0$. It is supposed that the crack length parameter is $c / h_1 = 0.1$, the crack location parameter is $(a+b)/2h_1 = 0.5$ and the nonhomogeneous parameter is $\beta h_1 = 0.0$. In the following figures, the time t is represented through the dimensionless Fourier number defined by

$$F = \frac{\tau_0 t}{h^2} \tag{28}$$

Note that the values of those intensity factors rise sharply at first, reach maximum values and then decrease and approach the static values with increasing F. The results for the case of $h_2 / h_1 \rightarrow 0.0$ are coincident with the results of the previous paper [3]. The magnitudes of $(K_{\mathrm{IA}},\, K_{\mathrm{IB}}) / \lambda_{110} T_0 (\pi c)^{1/2}$ depend remarkably on h_2 / h_1. The normalized maximum values of the stress intensity factors for $h_2 / h_1 = 0.5$ are larger than those for $h_2 / h_1 = 1.0$ and $h_2 / h_1 \rightarrow 0.0$.

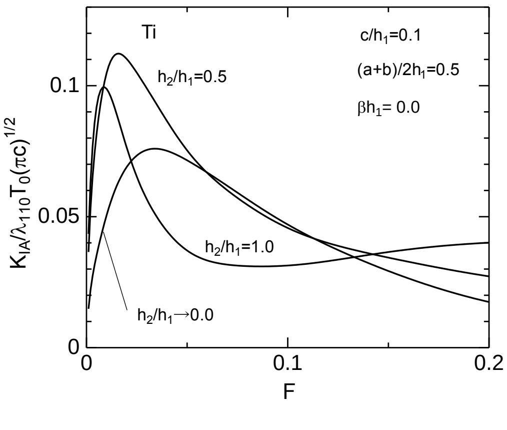

Figure 2(a). The effect of the thickness ratio h_2 / h_1 on the stress intensity factor K_{IA} for the Ti layer (embedded crack).

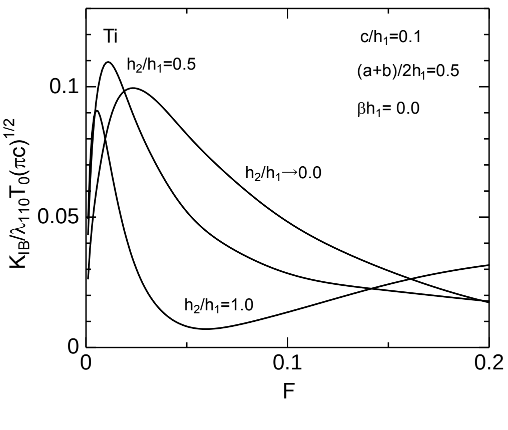

Figure 2(b). The effect of the thickness ratio h_2 / h_1 on the stress intensity factor K_{IB} for the Ti layer (embedded crack).

Next, we examine the effect of the crack length parameter c/h_1 on the time dependences of the stress intensity factors K_{IA} and K_{IB} for the Ti elastic layer. The normalized stress intensity factors $(K_{\mathrm{IA}},\, K_{\mathrm{IB}})/\lambda_{110}T_0(\pi c)^{1/2}$ are plotted versus F for $c/h_1 = 0.1$, 0.2 and 0.3 with $h_2/h_1 = 1.0$, $(a+b)/2h_1 = 0.5$ and $\beta h_1 = 2.0$ in Figures 3(a) and 3(b). The same tendencies as the cases shown in Figures 2(a) and 2(b) are observed. For the case of $c/h_1 = 0.3$, the value of $K_{\mathrm{IB}}/\lambda_{110}T_0(\pi c)^{1/2}$ at some time becomes negative, and the crack would be closed, because the stress $\sigma_0^T(z,t) \quad (a<z<b)$ on the surfaces of the crack becomes compressive.

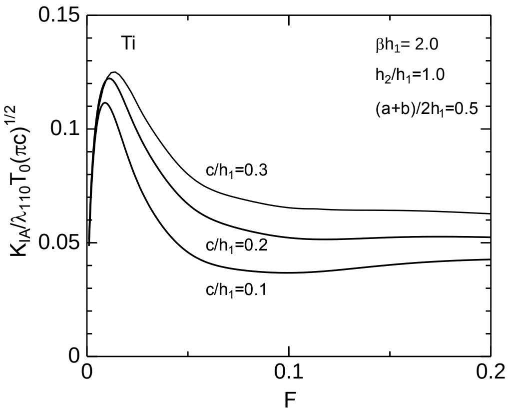

Figure 3(a). The effect of the crack length c/h_1 on the stress intensity factor K_{IA} for the Ti layer (embedded crack).

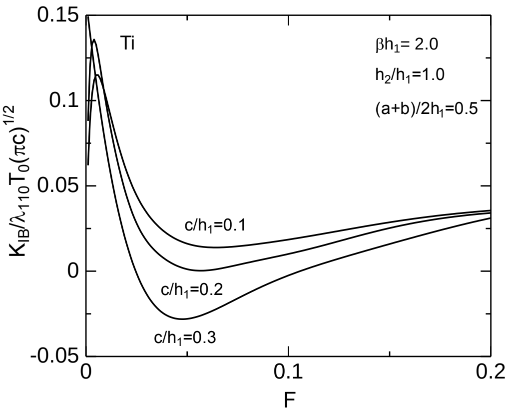

Figure 3(b). The effect of the crack length c/h_1 on the stress intensity factor K_{IB} for the Ti layer (embedded crack).

Thirdly, we consider the effect of the crack location parameter $(a+b)/2h_1$, the nonhomogeneous parameter βh_1 and the material properties of the elastic layer. Figures 4(a) and (b) indicate the time dependences of the stress intensity factors K_{IA} and K_{IB} for the Ti elastic layer. It is supposed that the geometric parameters are $c/h_1 = 0.1$, $h_2/h_1 = 1.0$ and $(a+b)/2h_1$=0.2, 0.5 and 0.8. In these figures, the solid, dashed and dotted lines indicate the results for the $\beta h_1 = 2.0$, -2.0 and 0.0, respectively. Figures 5(a) and (b) are the same as Figures 4(a) and (b) for the Brass elastic layer. For the case of $(a+b)/2h_1$=0.8, we can also see the crack contact phenomenon. The values of the stress intensity factors for the Brass layer are much larger than those for the Ti layer. The most remarkable difference between the results for the Ti elastic layer and the Brass layer is whether the time dependences of the stress intensity factors have the peak value or not. For the case of the Brass layer, the time dependences of $(K_{\mathrm{IA}},\ K_{\mathrm{IB}})/\lambda_{110}T_0(\pi c)^{1/2}$ do not have the peak value.

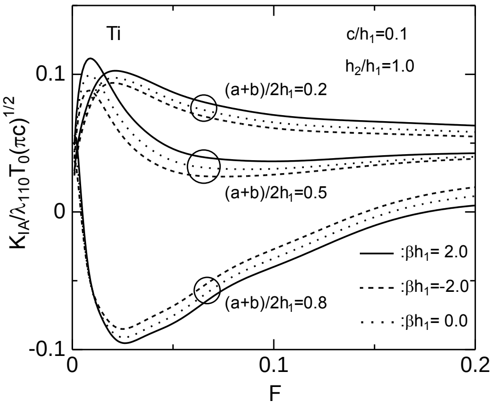

Figure 4(a). The effect of the crack location $(a+b)/2h_1$ and the nonhomogeneous parameter βh_1 on the stress intensity factor K_{IA} for the Ti layer (embedded crack).

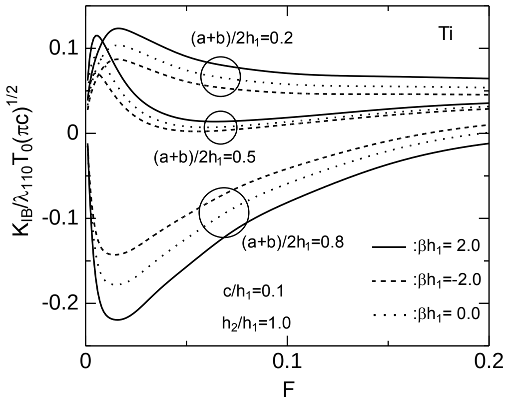

Figure 4(b). The effect of the crack location $(a+b)/2h_1$ and the nonhomogeneous parameter βh_1 on the stress intensity factor K_{IB} for the Ti layer (embedded crack).

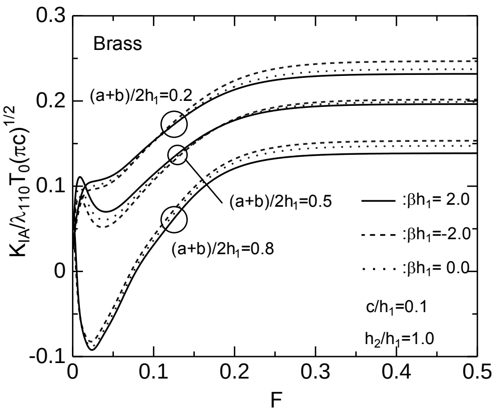

Figure 5(a). The effect of the crack location $(a+b)/2h_1$ and the nonhomogeneous parameter βh_1 on the stress intensity factor K_{IA} for the Brass layer (embedded crack).

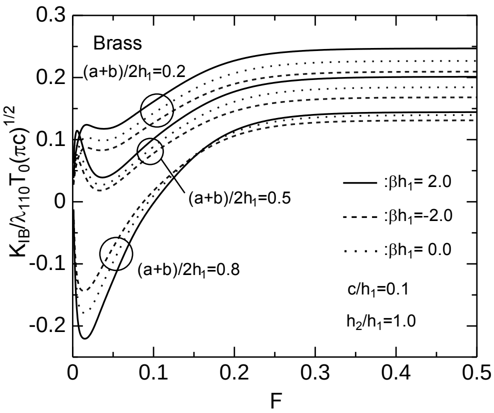

Figure 5(b). The effect of the crack location $(a+b)/2h_1$ and the nonhomogeneous parameter βh_1 on the stress intensity factor K_{IB} for the Brass layer (embedded crack).

Finally, we consider the case of $b = h_1$ (edge crack). Assume the top surface of the strip is cooled from initial temperature T_{I} to $T_{\mathrm{I}} + T_0$ $(T_0 < 0)$ suddenly, the normalized stress intensity factor $K_{\mathrm{IA}}/\lambda_{110}\,|T_0|\,(2\pi c)^{1/2}$ is plotted versus F for the $\beta h_1 = 2.0$, -2.0 and 0.0 with $2c/h_1 = 0.2$ in Figure 6 and for $2c/h_1 = 0.2, 0.4$ with $\beta h_1 = 2.0$ in Figure 7, respectively. The normalized value of stress intensity factor decreases with decreasing βh_1 and $2c/h_1$. The influence of the material nonhomogeneity on the stress intensity factor is the same as the results for the embedded crack shown in Figure 4(a). For the case of large F, the stress intensity factor may be negative and the crack contact occurs.

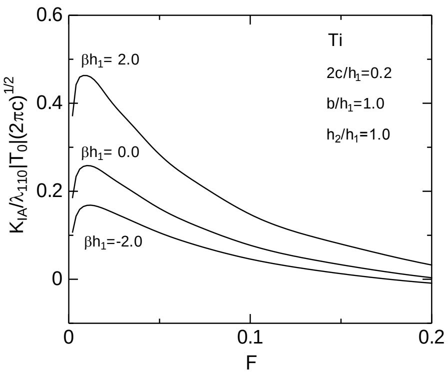

Figure 6. The effect of the nonhomogeneous parameter βh_1 on the stress intensity factor K_{IA} for the Ti layer (edge crack).

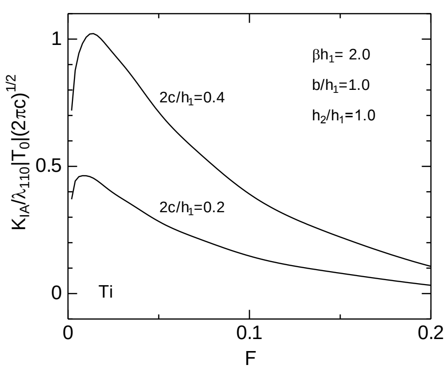

Figure 7. The effect of the crack length $2c/h_1$ on the stress intensity factor K_{IA} for the Ti layer (edge crack).

CONCLUSION

The transient fracture problem of the cracked functionally graded piezoelectric strip bonded to the homogeneous elastic layer is studied. The effects of the thickness of the elastic layer, the crack length, the crack location and the material nonhomogenity on the fracture behavior are considered. The following facts can be found from the numerical results.

(1) The distinct overshooting phenomenon for the case of the Ti elastic layer can be observed and this fact may suggest the importance of these transient analyses. The effect of the thickness of the elastic layer on the time dependence of the stress intensity factors is large (Figs. 2(a) and 2(b)).

(2) The maximum values of the stress intensity factors and the static values of them indicating the inertial effect increase with increasing c/h_1. For the case of $c/h_1 = 0.3$, the stress intensity factor K_{IB} becomes negative (Figs. 3(a) and 3(b)).

(3) While the time dependences of the stress intensity factors for the Ti elastic layer have the peak values, those for the Brass layer do not have the peak values. Generally, the decrease of βh_1 is beneficial for reducing the stress intensity factors. However, the static values of the stress intensity factors for the Brass elastic layer decreases with increasing βh_1. For the case of the crack near the heating surface, the crack contact phenomenon can be found (Figs. 4(a), 4(b) and 5(a), 5(b)).

(4) In some cases, the stress intensity factors under the thermal load become negative and the results have no physical meaning. However, when the thermal load is combined with the mechanical load which induces the positive stress intensity factor, those results can be used effectively.

Appendix A

The functions $\mu_{ij}\ (i, j = 1, 2)$ are

$$\left.\begin{aligned} \mu_{11} &= -\frac{\delta}{2} - \mu_0, \quad \mu_{21} = \left(\frac{p}{\tau_0^E}\right)^{1/2} \\ \mu_{12} &= -\frac{\delta}{2} + \mu_0, \quad \mu_{22} = -\left(\frac{p}{\tau_0^E}\right)^{1/2} \end{aligned}\right\} \tag{A.1}$$

where

$$\mu_0 = \left(\frac{\delta^2}{4} + \frac{p}{\tau_0}\right)^{1/2} \tag{A.2}$$

The functions D_{ij} $(i, j = 1, 2)$ are

$$\left.\begin{aligned}
D_{11} &= \frac{\rho_{01}\rho_{22}}{\rho_{11}\rho_{22} - \rho_{12}\rho_{21}} \frac{T_0}{p} \\
D_{21} &= -\frac{\rho_{01}\rho_{12}}{\rho_{11}\rho_{22} - \rho_{12}\rho_{21}} \frac{T_0}{p} \\
D_{12} &= \frac{\left(\rho_{11}\rho_{22} - \rho_{12}\rho_{21}\right)\exp\left(-\mu_{12}h_1\right) - \rho_{01}\rho_{22}\exp(-2\mu_0 h_1)}{\rho_{11}\rho_{22} - \rho_{12}\rho_{21}} \frac{T_0}{p} \\
D_{22} &= \frac{\rho_{01}\rho_{12}\exp(-2\mu_{21}h_2)}{\rho_{11}\rho_{22} - \rho_{12}\rho_{21}} \frac{T_0}{p}
\end{aligned}\right\} \tag{A.3}$$

where

$$\left.\begin{aligned}
\rho_{01} &= \left(\mu_{12} - \mu_{22}\right)\exp\left(-\mu_{12}h_1\right) \\
\rho_{02} &= \left(\mu_{12} - \mu_{22}\right)\exp\left(\mu_{22}h_2\right) \\
\rho_{11} &= \mu_{22} - \mu_{11} + \left(\mu_{12} - \mu_{22}\right)\exp\left(-2\mu_0 h_1\right) \\
\rho_{21} &= \mu_{21} - \mu_{22} \\
\rho_{12} &= \mu_{12} - \mu_{11} \\
\rho_{22} &= \mu_{21} - \mu_{12} + \left(\mu_{12} - \mu_{22}\right)\exp\left(-2\mu_{21}h_2\right)
\end{aligned}\right\} \tag{A.4}$$

Appendix B

The constant Z^∞ is given by

$$\left.\begin{aligned}
Z^\infty &= \lim_{s\to\infty} Z(s) \\
Z(s) &= \sum_{j=1}^{3} p_{11j}(s)\delta_j(s)
\end{aligned}\right\} \tag{B.1}$$

where

$$\left.\begin{aligned}
\delta_1(s) &= \frac{\rho_{22}(s)\rho_{33}(s)}{a_{11}(s)\rho_{22}(s)\rho_{33}(s) - a_{12}(s)\rho_{21}(s)\rho_{33}(s) - a_{13}(s)\rho_{22}(s)\rho_{31}(s)} \\
\delta_j(s) &= -\frac{\rho_{j1}(s)}{\rho_{jj}(s)}\delta_1(s) \quad (j = 2, 3)
\end{aligned}\right\} \tag{B.2}$$

with

$$\left.\begin{aligned}\rho_{2j}(s) &= p_{313}(s)p_{21j}(s) - p_{213}(s)p_{31j}(s)\\ \rho_{3j}(s) &= p_{312}(s)p_{21j}(s) - p_{212}(s)p_{31j}(s)\end{aligned}\right\} \quad (j = 2,3) \tag{B.3}$$

The kernel functions $M_i(\xi, z)$ $(i = 1,2,3,4)$ are

$$\left.\begin{aligned}M_1(\xi,z) &= \int_0^\infty \left[\frac{\Re[Z(s)]}{\Re[Z^\infty]} - 1\right]\sin[s(\xi - z)]ds\\ M_2(\xi,z) &= \int_0^\infty \frac{\Im[Z(s)]}{\Re[Z^\infty]}\cos[s(\xi - z)]ds\\ M_3(\xi,z) &= -\frac{2}{\Re[Z^\infty]}\int_0^\infty m^\infty(s,\xi,z)ds\\ M_4(\xi,z) &= -\frac{2}{\Re[Z^\infty]}\int_0^\infty \left[m(s,\xi,z) - m^\infty(s,\xi,z)\right]ds\end{aligned}\right\} \tag{B.4}$$

where

$$\left.\begin{aligned}m(s,\xi,z) &= \sum_{i=1}^{8}\sum_{j=1}^{3} p_{12j}(s)r_{ji}(s)Q_i(s,\xi)\exp(s\gamma_{2j}z)\\ &\quad + \sum_{i=1}^{8}\sum_{j=4}^{6} p_{12j}(s)r_{ji}(s)Q_i(s,\xi)\exp[-s\gamma_{2j}(h_1 - z)]\\[1em] m^\infty(s,\xi,z) &= \sum_{k=1}^{3}\left\{\sum_{i=1}^{3} p^\infty_{i+2,1k}\left[\sum_{j=1}^{3} F_{ijk}\exp(-s\theta_{1jk}) + \sum_{j=4}^{6} F_{ijk}\exp(-s\theta_{3jk})\right]\right.\\ &\quad + \sum_{i=4}^{6} p^\infty_{i-1,1k}\left[\sum_{j=1}^{3} F_{ijk}\exp(-s\theta_{2jk}) + \sum_{j=4}^{6} F_{ijk}\exp(-s\theta_{4jk})\right]\\ &\quad \left. + \sum_{i=7}^{8} p^\infty_{i-1,1k}\left[\sum_{j=1}^{3} \bar{F}_{ijk}\exp(-s\theta_{1jk}) + \sum_{j=4}^{6} \bar{F}_{ijk}\exp(-s\theta_{3jk})\right]\right\}\end{aligned}\right\} \tag{B.5}$$

$$\left.\begin{aligned}
F_{ijk} &= \frac{1}{2\gamma_{1k}^{\infty}} p_{12j}^{\infty} r_{ji}^{\infty} \delta_k^{\infty} && (i, j = 1, 2, \ldots, 6) \\
\bar{F}_{ijk} &= \frac{1}{2} p_{12j}^{\infty} r_{ji}^{\infty} \delta_k^{\infty} && (i = 7, 8,\ j = 1, 2, \ldots, 6) \\
\theta_{1jk} &= -\frac{\xi}{\gamma_{1k}^{\infty}} - \gamma_{2j}^{\infty} z && (j = 1, 2, 3) \\
\theta_{2jk} &= -\frac{h_1 - \xi}{\gamma_{1k}^{\infty}} - \gamma_{2j}^{\infty} z && (j = 1, 2, 3) \\
\theta_{3jk} &= -\frac{\xi}{\gamma_{1k}^{\infty}} - \gamma_{2j}^{\infty} (h_1 - z) && (j = 4, 5, 6) \\
\theta_{4jk} &= -\frac{h_1 - \xi}{\gamma_{1k}^{\infty}} - \gamma_{2j}^{\infty} (h_1 - z) && (j = 4, 5, 6)
\end{aligned}\right\} (k = 1, 2, 3) \tag{B.6}$$

$$\left.\begin{aligned}
p_{i1j}^{\infty} &= \lim_{s\to\infty} p_{i1j}(s) && (i = 1, 2, \ldots, 8,\quad j = 1, 2, 3) \\
p_{i2j}^{\infty} &= \lim_{s\to\infty} p_{i2j}(s) && (i = 1, 2, \ldots, 8,\quad j = 1, 2, \ldots, 6) \\
r_{ji}^{\infty} &= \lim_{s\to\infty} r_{ji}(s) && (i, j = 1, 2, \ldots, 10) \\
\gamma_{1j}^{\infty} &= \lim_{s\to\infty} \gamma_{1j}(s) && (j = 1, 2, 3) \\
\gamma_{2j}^{\infty} &= \lim_{s\to\infty} \gamma_{2j}(s) && (j = 1, 2, \ldots, 6) \\
\delta_j^{\infty} &= \lim_{s\to\infty} \delta_j(s) && (j = 1, 2, 3)
\end{aligned}\right\} \tag{B.7}$$

where

$$\left.\begin{aligned}
p_{11j}(s) &= c_{110}\gamma_{1j} a_{1j}(s) - c_{130} - e_{310} b_{1j}(s) \\
p_{21j}(s) &= e_{150}[\gamma_{1j} + a_{1j}(s)] - \varepsilon_{110}\gamma_{1j} b_{1j}(s) \\
p_{31j}(s) &= c_{440}[\gamma_{1j} + a_{1j}(s)] + e_{150}\gamma_{1j} b_{1j}(s) \\
p_{41j}(s) &= c_{130}\gamma_{1j} a_{1j}(s) - c_{330} - e_{330} b_{1j}(s) \\
p_{51j}(s) &= e_{310}\gamma_{1j} a_{1j}(s) - e_{330} + \varepsilon_{330} b_{1j}(s) \\
p_{61j}(s) &= a_{1j}(s) \\
p_{71j}(s) &= 1 \\
p_{81j}(s) &= b_{1j}(s)
\end{aligned}\right\} \quad (j = 1, 2, 3) \tag{B.8}$$

$$\left.\begin{aligned}
p_{12j}(s) &= c_{110}a_{2j}(s) - \gamma_{2j}[c_{130} - e_{310}b_{2j}(s)] \\
p_{22j}(s) &= e_{150}[\gamma_{2j}a_{2j}(s) - 1] - \varepsilon_{110}b_{2j}(s) \\
p_{32j}(s) &= c_{440}[\gamma_{2j}a_{2j}(s) - 1] + e_{150}b_{2j}(s) \\
p_{42j}(s) &= c_{130}a_{2j}(s) + \gamma_{2j}[c_{330} - e_{330}b_{2j}(s)] \\
p_{52j}(s) &= e_{310}a_{2j}(s) + \gamma_{2j}[e_{330} + \varepsilon_{330}b_{2j}(s)] \\
p_{62j}(s) &= a_{2j}(s) \\
p_{72j}(s) &= 1 \\
p_{82j}(s) &= -b_{2j}(s)
\end{aligned}\right\} \quad (j = 1, 2, ..., 6) \qquad \text{(B.9)}$$

In Eqs. (B.2), (B.7), (B.8) and (B.9), the functions $\gamma_{1j} = \gamma_{1j}(s)$, $a_{1j}(s)$ and $b_{1j}(s)$ $(j = 1, 2, 3)$ are given in Appendix A of the previous paper [7], and the functions $\gamma_{2j} = \gamma_{2j}(s)$, $a_{2j}(s)$ and $b_{2j}(s)$ $(j = 1, 2, ..., 6)$ are given in Appendix B of the previous paper [4].The functions $r_{ij}(s)$ $(i, j = 1, 2, ..., 10)$ are the elements of a square matrix $R = \Omega^{-1}$ of order 10. The elements $\omega_{i,j}(s)$ $(i, j = 1, 2, ..., 10)$ of the square matrix Ω are given by

$$\left.\begin{aligned}
\omega_{i-2,j}(s) &= p_{i2j}(s) && (i = 3, 4, 5) \\
\omega_{i+1,j}(s) &= p_{i2j}(s)\exp(s\gamma_{2j}h_1) && (i = 3, 4, 5) \\
\omega_{i+1,j}(s) &= p_{i2j}(s) && (i = 6, 7)
\end{aligned}\right\} (j = 1, 2, ..., 6) \qquad \text{(B.10)}$$

$$\left.\begin{aligned}
&\omega_{1,7}(s) = 2\mu, && \omega_{1,8}(s) = 2\mu(1-2\nu) \\
&\omega_{1,9}(s) = -2\mu, && \omega_{1,10}(s) = 2\mu(1-2\nu) \\
&\omega_{2,7}(s) = 2\mu, && \omega_{2,8}(s) = 2\mu(1-\nu) \\
&\omega_{2,9}(s) = 2\mu, && \omega_{2,10}(s) = -2\mu(1-\nu) \\
&\omega_{7,7}(s) = -1, && \omega_{7,9}(s) = -1 \\
&\omega_{8,7}(s) = -1, && \omega_{8,8}(s) = -(3-4\nu) \\
&\omega_{8,9}(s) = 1, && \omega_{8,10}(s) = -(3-4\nu) \\
&\omega_{9,7}(s) = \exp(sh_2), && \omega_{9,8}(s) = -(sh_2 - 1 + 2\nu)\exp(sh_2) \\
&\omega_{9,9}(s) = -\exp(-sh_2), && \omega_{9,10}(s) = (sh_2 + 1 - 2\nu)\exp(-sh_2) \\
&\omega_{10,7}(s) = \exp(sh_2), && \omega_{10,8}(s) = -(sh_2 - 2 + 2\nu)\exp(sh_2) \\
&\omega_{10,9}(s) = \exp(-sh_2), && \omega_{10,10}(s) = -(sh_2 + 2 - 2\nu)\exp(-sh_2)
\end{aligned}\right\} \qquad \text{(B.11)}$$

The functions $Q_i(s,\xi)(i=1,2,...,6)$ are

$$Q_1(s,\xi)=\frac{1}{2}\sum_{j=1}^{3}\Re\left[\frac{p_{31j}^{\infty}\delta_j^{\infty}}{\gamma_{1j}^{\infty}}\exp\left(\frac{s\xi}{\gamma_{1j}^{\infty}}\right)\right]$$
$$-\frac{s}{\pi}\sum_{j=1}^{3}\int_0^{\infty}\left\{\begin{array}{l}\Re\left[\dfrac{p_{31j}\delta_j}{\gamma_{1j}^2}\dfrac{1}{\eta^2+(s/\gamma_{1j})^2}\right]\\ -\Re\left[\dfrac{p_{31j}^{\infty}\delta_j^{\infty}}{\gamma_{1j}^{\infty 2}}\dfrac{1}{\eta^2+(s/\gamma_{1j}^{\infty})^2}\right]\end{array}\right\}\cos(\eta\xi)d\eta \tag{B.12}$$
$$+\frac{s}{\pi}\sum_{j=1}^{3}\int_0^{\infty}\Im\left[\frac{p_{31j}\delta_j}{\gamma_{1j}^2}\frac{1}{\eta^2+(s/\gamma_{1j})^2}\right]\sin(\eta\xi)d\eta$$

$$Q_{k-2}(s,\xi)=\frac{1}{2}\sum_{j=1}^{3}\Re\left[\frac{p_{k1j}^{\infty}\delta_j^{\infty}}{\gamma_{1j}^{\infty}}\exp\left(\frac{s\xi}{\gamma_{1j}^{\infty}}\right)\right]$$
$$+\frac{1}{\pi}\sum_{j=1}^{3}\int_0^{\infty}\eta\left\{\begin{array}{l}\Re\left[\dfrac{p_{k1j}\delta_j}{\gamma_{1j}^2}\dfrac{1}{\eta^2+(s/\gamma_{1j})^2}\right]\\ -\Re\left[\dfrac{p_{k1j}^{\infty}\delta_j^{\infty}}{\gamma_{1j}^{\infty 2}}\dfrac{1}{\eta^2+(s/\gamma_{1j}^{\infty})^2}\right]\end{array}\right\}\sin(\eta\xi)d\eta \tag{B.13}$$
$$+\frac{1}{\pi}\sum_{j=1}^{3}\int_0^{\infty}\eta\Im\left[\frac{p_{k1j}\delta_j}{\gamma_{1j}^2}\frac{1}{\eta^2+(s/\gamma_{1j})^2}\right]\cos(\eta\xi)d\eta \quad (k=4,5)$$

$$Q_4(s,\xi)=\frac{1}{2}\sum_{j=1}^{3}\Re\left[\frac{p_{31j}^{\infty}\delta_j^{\infty}}{\gamma_{1j}^{\infty}}\exp\left(\frac{s(h_1-\xi)}{\gamma_{1j}^{\infty}}\right)\right]$$
$$-\frac{s}{\pi}\sum_{j=1}^{3}\int_0^{\infty}\left\{\begin{array}{l}\Re\left[\dfrac{p_{31j}\delta_j}{\gamma_{1j}^2}\dfrac{1}{\eta^2+(s/\gamma_{1j})^2}\right]\\ -\Re\left[\dfrac{p_{31j}^{\infty}\delta_j^{\infty}}{\gamma_{1j}^{\infty 2}}\dfrac{1}{\eta^2+(s/\gamma_{1j}^{\infty})^2}\right]\end{array}\right\}\cos[\eta(h_1-\xi)]d\eta \tag{B.14}$$
$$-\frac{s}{\pi}\sum_{j=1}^{3}\int_0^{\infty}\Im\left[\frac{p_{31j}\delta_j}{\gamma_{1j}^2}\frac{1}{\eta^2+(s/\gamma_{1j})^2}\right]\sin[\eta(h_1-\xi)]d\eta$$

$$Q_{k+1}(s,\xi)=\frac{1}{2}\sum_{j=1}^{3}\Re\left[\frac{p_{k1j}^{\infty}\delta_j^{\infty}}{\gamma_{1j}^{\infty}}\exp\left(\frac{s(h_1-\xi)}{\gamma_{1j}^{\infty}}\right)\right]$$
$$+\frac{1}{\pi}\sum_{j=1}^{3}\int_0^{\infty}\eta\left\{\begin{array}{l}\Re\left[\dfrac{p_{k1j}\delta_j}{\gamma_{1j}^2}\dfrac{1}{\eta^2+(s/\gamma_{1j})^2}\right]\\ -\Re\left[\dfrac{p_{k1j}^{\infty}\delta_j^{\infty}}{\gamma_{1j}^{\infty 2}}\dfrac{1}{\eta^2+(s/\gamma_{1j}^{\infty})^2}\right]\end{array}\right\}\sin[\eta(h_1-\xi)]d\eta \tag{B.15}$$
$$-\frac{1}{\pi}\sum_{j=1}^{3}\int_0^{\infty}\eta\Im\left[\frac{p_{k1j}\delta_j}{\gamma_{1j}^2}\frac{1}{\eta^2+(s/\gamma_{1j})^2}\right]\cos[\eta(h_1-\xi)]d\eta\quad (k=4,5)$$

$$Q_7(s,\xi)=\frac{1}{2}\sum_{j=1}^{3}\Re\left[p_{61j}^{\infty}\delta_j^{\infty}\exp\left(\frac{s\xi}{\gamma_{1j}^{\infty}}\right)\right]$$
$$-\frac{s^2}{\pi}\sum_{j=1}^{3}\int_0^{\infty}\frac{1}{\eta}\left\{\begin{array}{l}\Re\left[\dfrac{p_{61j}\delta_j}{\gamma_{1j}^2}\dfrac{1}{\eta^2+(s/\gamma_{1j})^2}\right]\\ -\Re\left[\dfrac{p_{61j}^{\infty}\delta_j^{\infty}}{\gamma_{1j}^{\infty 2}}\dfrac{1}{\eta^2+(s/\gamma_{1j}^{\infty})^2}\right]\end{array}\right\}\sin(\eta\xi)d\eta \tag{B.16}$$
$$-\frac{s^2}{\pi}\sum_{j=1}^{3}\int_0^{\infty}\frac{1}{\eta}\Im\left[\frac{p_{61j}\delta_j}{\gamma_{1j}^2}\frac{1}{\eta^2+(s/\gamma_{1j})^2}\right]\cos(\eta\xi)d\eta$$

$$Q_8(s,\xi)=\frac{1}{2}\sum_{j=1}^{3}\Re\left[\frac{p_{71j}^{\infty}\delta_j^{\infty}}{\gamma_{1j}^{\infty}}\exp\left(\frac{s\xi}{\gamma_{1j}^{\infty}}\right)\right]$$
$$-\frac{s}{\pi}\sum_{j=1}^{3}\int_0^{\infty}\left\{\begin{array}{l}\Re\left[\dfrac{p_{71j}\delta_j}{\gamma_{1j}}\dfrac{1}{\eta^2+(s/\gamma_{1j})^2}\right]\\ -\Re\left[\dfrac{p_{71j}^{\infty}\delta_j^{\infty}}{\gamma_{1j}^{\infty}}\dfrac{1}{\eta^2+(s/\gamma_{1j}^{\infty})^2}\right]\end{array}\right\}\cos(\eta\xi)d\eta \tag{B.17}$$
$$+\frac{s}{\pi}\sum_{j=1}^{3}\int_0^{\infty}\Im\left[\frac{p_{71j}\delta_j}{\gamma_{1j}}\frac{1}{\eta^2+(s/\gamma_{1j})^2}\right]\sin(\eta\xi)d\eta$$

References

[1] Wu, C. M., Kahn, M. and Moy, W. (1996) Piezoelectric Ceramics with Functionally Gradients : A New Application in Material Design, *Journal of American Ceramics Society*, Vol.79, pp.809-812.

[2] Wang, B. L. and Noda, N. (2001) Thermally Induced Fracture of a Smart Functionally Graded Composite Structure, *Theoretical and Applied Fracture Mechanics*, Vol.35, pp.93-109.

[3] Ueda, S. (2004) Thermally Induced Fracture of a Functionally Graded Piezoelectric Layer, *Journal of Thermal Stresses,* Vol.27, pp.291-309.

[4] Ueda, S. (2007) Thermal Intensity Factors for a Parallel Crack in a Functionally Graded Piezoelectric Strip, *Journal of Thermal Stresses,* Vol.30, pp.321-342.

[5] Ueda, S. (2007) A Penny-Shaped Crack in a Functionally Graded Piezoelectric Strip under Thermal Loading, *Engineering Fracture Mechanics,* Vol.74, pp.1255-1273.

[6] Ueda, S. and Kondo, H. (2008) Transient Intensity Factors for a Parallel Crack in a Plate of a Functionally Graded Piezoelectric Material under Thermal Shock Loading Conditions, *Journal of Thermal Stresses,* Vol.31, pp.211-232.

[7] Ueda, S. (2008) A Cracked Functionally Graded Piezoelectric Material Strip under Transient Thermal Loading, *Acta Mechanica*, Vol.199, pp.53-70.

[8] Ueda, S. (2008) Transient Thermoelectroelastic Response of a Functionally Graded Piezoelectric Strip with a Penny-Shaped Crack, *Engineering Fracture Mechanics,* Vol.75, pp.1204-1222.

[9] Wang, B. L. and Mai, Y.-W. (2002) A Cracked Piezoelectric Material Strip under Transient Thermal Loading, *Transactions of the ASME, Journal of Applied Mechanics*, Vol.69, pp.539-546.

[10] Ueda, S. (2006) Transient Response of a Cracked Piezoelectric Strip under Thermoelectric Loading, *Journal of Thermal Stresses,* Vol.29, pp.973-994.

[11] Uchino, K., Yoshizaki, M., Kasai, K., Yamamura, H., Sakai, N. and Asakura, H. (1987) Monomorph Actuators using Semiconductive Ferroelectrics, *Japan Journal of Applied Physics*, Vol.26, pp.1046-1049.

[12] Miller, M. K. and Guy, W. T. (1966) Numerical Inversion of the Laplace Transform by Use of Jacobi Polynomials, SIAM *Journal of Numerical Analysis,* vol. 3, pp. 624-635.

[13] Sneddon, I. N. and Lowengrub, M. (1969) *Crack Problems in the Classical Theory of Elasticity*, John Wiley & Sons, Inc., New York.

[14] Erdogan, F. and Wu, B. H. (1996) Crack Problems in FGM Layers Under Thermal Stresses, *Journal of Thermal Stresses,* vol. 19, pp. 237-265.

[15] Erdogan, F., Gupta, G. D. and Cook, T. S. (1972) *Methods of Analysis and Solution of Crack Problems*, in G. C. Sih (ed), Noordhoff, Leyden.

[16] Ashida, F. and Tauchert, T. R. (1998) Transient Response of a Piezothermoelastic Circular Disk Under Axisymmetric Heating, *Acta Mechanica*, vol. 128, pp. 1-14.